



OPEN

Optimization of Cd (II) removal from aqueous solution by natural hydroxyapatite/bentonite composite using response surface methodology

Yiene Molla Desalegn^{1✉}, Endrias Adane Bekele² & Femi Emmanuel Olu²

Toxic cadmium (Cd) was removed from water using eggshell-based hydroxyapatite (HAp) grafted bentonite (HAp/bentonite) composite through a straightforward chemical synthesis route. The as-prepared adsorbents were characterized using X-ray diffraction (XRD), scanning electron microscopy (SEM), Fourier transform infrared spectroscopy (FTIR), and Brunauer–Emmett–Teller analysis (BET). Optimization of the initial adsorbate concentration, adsorbent dosage, pH, and contact time—all of which affect the adsorption process—was performed using the central composite design (CCD) of the response surface methodology (RSM). 99.3 percent adsorptive removal efficiency was observed at an initial concentration of 61.58 mg/L of Cd (II), with an adsorbent dosage of 1.58 g, a solution pH of 5.88, and a contact time of 49.63 min. The analysis of variance (ANOVA) was performed, and the multiple correlation coefficient (R^2) was found to be 0.9915 which confirms the significance of the predicted model. The Langmuir isotherm model best represented the adsorption isotherm data, which also predicted a maximum sorption capacity of 125.47 mg/g. The kinetic data were best described by the pseudo-second order model.

Heavy metal ion pollution of water is now the most concerning environmental problem because of its devastating effects on both nature and humans. Lead (Pb), copper (Cu), cadmium (Cd), chromium (Cr), mercury (Hg), arsenic (As), zinc (Zn), and nickel (Ni) are all examples of heavy metals because their densities are higher than 5 g/cm³^{1–3}. Electroplating, metallurgy and mining, agriculture, dying, coking, pharmaceuticals, and nickel–cadmium batteries are just some of the industries and products that release toxic heavy metals into the environment⁴. Cd(II) is the most important of these⁵. Cd(II) is readily absorbed by ecosystems and then accumulates in people through the food chain, where it has been linked to cancer, hypertension, renal dysfunction, and liver disorders⁶. Potable water should not contain more than 0.003 mg/L of Cd(II), as recommended by the World Health Organization^{7,8}. For obvious reasons, heavy metal contaminants in aqueous solutions must be eliminated using appropriate technologies, such as adsorption, coagulation, flocculation, ion exchange, bioremediation, and membrane separation⁹. Adsorption stands out as the best treatment option because of its low cost, high selectivity, high efficiency, and lack of hazardous byproducts^{10,11}.

Recently, clays have drawn the attention of environmental researchers due to their availability, cost-effectiveness, and chemical and mechanical stability¹². For application in heavy metal removal from wastewater, the clay needs to possess a large surface area, chemical stability, and high cation exchange capacity^{13,14}. Due to its large specific surface area and relatively high cation-exchange capacity, bentonite was considered an efficient adsorbent in the removal of various heavy metal ions.

Hend et al. (2016) evaluated the application of nano-bentonite to remove Pb(II) and Cd(II) from an aqueous solution. The results revealed that the adsorption behavior of Pb(II) and Cd(II) onto nano-bentonite was best described with the Langmuir isotherm model, with a maximum adsorption capacity of 67 and 83 mg/g, respectively¹⁵.

¹Department of Mechanical Engineering, School of Mechanical and Chemical Engineering, Woldia Institute of Technology, Woldia University, Woldia, Ethiopia. ²Faculty of Materials Science and Engineering, Jimma Institute of Technology, Jimma University, Jimma, Ethiopia. ✉email: yiene21ayl@gmail.com

Şahan (2019) used bentonite enriched with SH groups (BSH) to remove Pb(II) and Cd(II) ions. In this study, the effect of different input variables (pH, initial metals concentration, adsorbent dosage, and contact time) on the removal efficiency was estimated. The optimal condition for pH, initial concentration, adsorbent dosage, and contact time was 5.10, 32.98 mg/L, 146 mg, and 146.01 min. for Pb(II), while these values were 4.52, 37.9 mg/L, 152.3 mg, and 146.12 min for Cd(II), respectively. At the optimum values, maximum Pb(II) and Cd(II) removal were obtained as 95.05% and 91.4%, respectively¹⁶.

In another study, Zhou et al. (2019) developed amino-functionalized bentonite/CoFe₂O₄@MnO₂ for the adsorption of Cd(II). The results revealed that the maximal adsorption efficiency for Cd(II) was found to be 98.88%. Moreover, The equilibrium adsorption isotherm showed that Langmuir isotherm fitted well to the experimental data with a maximum adsorption capacity of 115.79 mg/g¹⁷. However, the adsorption capacity of bentonite towards heavy metals ion may be limited by a lack of surface functional groups.

Over the past decades, apatite minerals like hydroxyapatite (HAp, Ca₁₀(PO₄)₆(OH)₂), has attracted huge interest in effectively adsorbing heavy metals ion^{18,19}. Some previous studies investigated HAp for the removal of a variety of contaminants. Nuñez et al. (2019) studied the adsorptive removal of heavy metals ions using HAp, and the highest adsorption capacities were found to be 265, 64, and 55 mg/g for Pb(II), Cd(II), and Cu(II), respectively²⁰. It is worth mentioning that the high ion exchange capacity and the ability to form a dissolution–precipitation reaction leads HAp to be one of the most competitive adsorbents in wastewater treatment²¹. Despite these interesting attributes, the high surface activity of HAp nanoparticles can lead to the formation of aggregates in aqueous solutions due to van der Waal's forces, which lowers the surface area and hinder the practical application of HAp for removing heavy metals from wastewater²². Furthermore, the application of synthetic HAp for wastewater treatment is constrained by its relatively high production cost^{23–25}. Therefore, studies are urgently needed on the improvement of HAp with a large surface area for adsorptive removal of Cd(II) from water. In this regard, bentonite clay can improve the surface area and cation-exchange capability, which in turn facilitates the reaction of HAp towards Cd(II)²⁶.

Hence, in this study, a new composite from eggshell-based HAp and bentonite was developed by a simple chemical synthesis route using glutaraldehyde as a cross-linking agent. The entire synthesis process was conducted under mild experimental conditions without using specialized equipment while consuming easily available and cost-effective starting reagents. Specifically, compared with the chemical reagents, eggshell had the significant advantage of being the cheapest source of hydroxyapatite. besides, effective re-utilization of waste materials for decontamination of water is also the basic principle of waste recycling.

Additionally, in the traditional method of analyzing the adsorption process, the interactive effect of process parameters on each other is not considered i.e., only one parameter is changed, and the other parameters are kept constant at a non-optimal level, which results in a cost and time-consuming and tedious optimization process. In this connection, the response surface methodology (RSM) was utilized, which is based on a set of statistical and mathematical techniques to design the experimental runs. Moreover, statistical optimization of operating parameters such as the initial adsorbate concentration, adsorbent dosage, pH, and contact time was conducted using a central composite design (CCD) of response surface methodology (RSM). The adsorption kinetics and isotherm modeling were also investigated to analyze the adsorption mechanism.

Experimental

Chemicals and reagents. All chemicals and reagents such as the phosphoric acid (H₃PO₄, 85%), ammonium hydroxide (NH₄OH), sodium hydroxide (NaOH, 99.8), glutaraldehyde (C₅H₈O₂, 25%), and cadmium chloride (CdCl₂, 99%) were used in this experiment without any further purification. Bentonite powder was purchased from Alkane Chemicals P.L.C (Addis Ababa, Ethiopia) and the eggshell was collected from the students' cafeteria of Jimma University (Jimma, Ethiopia). All the solutions were prepared using Distilled water.

Hydroxyapatite (HAp) preparation. HAp extracted from eggshell is environmentally friendly and cost-effective. HAp was extracted from eggshell by wet chemical precipitation method according to a procedure we reported elsewhere²⁷. Figure 1 shows an overall extraction process of HAp from the eggshell.

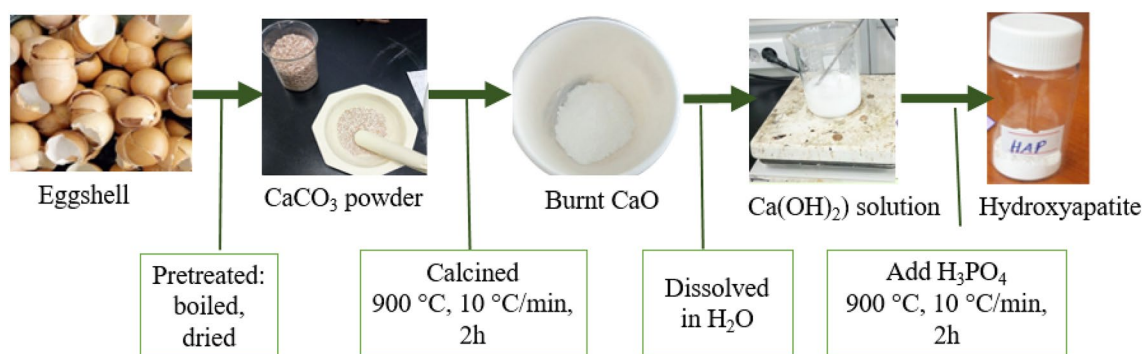


Figure 1. Synthesis steps of HAp from the eggshell.

Synthesis of Bentonite/hydroxyapatite composite. In a particular method, 0.5 g HAp and 0.5 g bentonite were added in different beakers (250 mL) containing distilled water and stirred at room temperature for 10 h to produce a homogeneous suspension. HAp solution was then poured into the bentonite clay solution under continuous stirring. Then, 50 mL of glutaraldehyde was added dropwise to the mixture to form crosslinking between the hydroxyl and the aldehyde groups. Then, the (0.1N) HCl solution was added dropwise to hold the pH at about 3 and stirred for 12 h. The obtained product was washed with distilled water and ethanol until the pH of the solution became neutral and then dried at a temperature of 60 °C overnight.

Characterization of the adsorbents. Shimadzu XRD- 7000 was used to analyze the phase purity of the adsorbents. Scanning electron microscopy (SEM, COXIEM-30, Shimadzu) was used for surface morphology characterization. The functional groups of the samples were characterized using Fourier-transform infrared spectroscopy (FT/IR-4000 series, JASCO). The textural properties of the adsorbent were measured by Brunauer–Emmett–Teller (BET) using a Quantachrome analyzer (Nova station C, version 11.0) based on the principle of adsorption/desorption of nitrogen at 77.3 K and 60/60 s (ads/des) equilibrium time.

Optimization of removal of cadmium using RSM: ANOVA result. The experiments were carried out to optimize the selected input variables such as initial concentration of Cd (II), adsorbent dosage, solution pH, and contact time and further investigate their interactive effects on the adsorption efficiency of Cd (II) from aqueous solution onto bentonite/HAp composite. All statistical analyses for the optimization of experimental studies were performed using CCD under RSM.

The number of experiments required for a total of four parameters was determined from the following equation:

$$N = 2^n + 2n + n_c \quad (1)$$

where N is the total number of experiments required, n is the number of factors, and n_c is the center point. Since a total of 30 experimental runs were conducted in this work, $2^4 = 16$ cube points, six replications at the center point, and eight axial points. Table 1 shows the level of chosen input variables and experimental ranges for Cd (II) removal efficiency (η).

The obtained experimental data were analyzed using Design expert 13.0 software, and the response variable (η) was correlated with four input factors by using the following quadratic polynomial equation:

$$\eta = a_0 + \sum_{j=1}^4 a_j Y_j + \sum_{j=1}^4 a_{jj} Y_j^2 + \sum_I \sum_{<j=2}^4 a_{ji} Y_i Y_j + e_i \quad (2)$$

where η is the response (removal efficiency for Cd (II)); Y_i and Y_j refer to variables (i and j range from 1 to k); a_0 refers to the coefficient of intercept; a_j , a_{jj} , and a_{ij} are known to be coefficients of interaction for the variables, respectively; and e_i is the error.

Cadmium adsorption experiments. The adsorption experiment was carried out in batch mode. The synthetic solutions at different concentrations were prepared by diluting the standard Cd solution (1000 mg/L) obtained by dissolving CdCl₂ in distilled water at room temperature. A sample of 20 mL volume adsorbate solution of specified initial concentrations (25–125 ppm) was shaken at 250 rpm at 25 °C using 1.25 g/L of the adsorbents (HAp/bentonite composite) in a 100 mL conical flask. Then, the samples were filtered using Whatman filter paper qualitative circles (125 nm \varnothing \times 100 circles) and analyzed the filtrates by an atomic absorption spectrometer (ZEE nit 700P, Atomic Flame Mode, Analytik Jena). All tests were carried out with repeatability, and their mean values were used in analyzing the data. The removal efficiency (η) was calculated using the following equation¹³.

$$\eta = \frac{(C_o - C_t)}{C_o} \times 100 \quad (3)$$

The adsorption capacity q_e (mg/g) of the adsorbent was calculated according to the following equation.

$$q_e = \frac{(C_o - C_t)V}{m} \quad (4)$$

Variables	Variable coding	Units	-alpha	Low	Center point	High	+ alpha
Initial Cd (II) conc	A	mg/L	25	50	75	100	125
Adsorbent dosage	B	g/L	0.25	0.75	1.25	1.75	2.25
pH	C	–	4.5	5	5.5	6	6.5
Contact time	D	min	30	40	50	60	70

Table 1. Levels of the adsorption process parameters considered.

where C_o (mg/L) is the initial concentration and C_e (mg/L) is the concentration of Cd (II) at equilibrium time. V (L) is the volume of the solution, and m (g) is the adsorbent mass.

Adsorption isotherm analysis. In this study, the applicability of isotherm models (Freundlich and Langmuir) was tested to select the most fitting model that would best describe and predict the adsorption of Cd (II) onto HAp/bentonite.

The Freundlich isotherm was based on the assumptions of the monolayer adsorption process with heterogeneous surface energy: the adsorbed species interact with one another²⁸. The well-known equation of this model can be given by the following equation²⁹:

$$\ln q_e = \ln K_F + \frac{1}{n} \ln C_e \quad (5)$$

where K_F is the Freundlich constant which implies the affinity of the heterogeneous surface towards the adsorbent and $1/n$ verifies the favorability of the adsorption process.

The Langmuir isotherm model assumes that the adsorption occurs on homogeneous surfaces without interaction between the adsorbed Cd (II)³⁰, and can be expressed according to the following Eq. (6) below.

$$\frac{C_e}{q_e} = \frac{1}{q_{max}b} + \frac{1}{q_{max}} C_e \quad (6)$$

where q_{max} (mg/g) is the monolayer adsorption capacity of the adsorbent, b (1/mg) is the Langmuir adsorption constant represents the affinity of the binding site.

Isotherms parameters for the two models were estimated from the slope and intercept of Eqs. (5) and (6) and listed in Table 6.

The favorability of Langmuir isotherm can be described by separation factor (R_L) whether it is favorable ($0 < R_L < 1$), unfavorable ($R_L > 1$), irreversible ($R_L = 0$), or linear ($R_L = 1$) as described in the following Eq. 7:

$$R_L = \frac{1}{1 + bC_o} \quad (7)$$

where C_o (mg/L) is the maximum initial Cd concentration and b (L/mg) is the Langmuir equilibrium constant³¹.

Kinetic modeling. The pseudo-first-order model, pseudo-second-order model, intraparticle diffusion model, and double constant equation model were considered to investigate the reaction order and mechanism of the adsorption process. These models were calculated according to Eqs. (8–11), respectively^{32,33}.

$$\log(q_e - q_t) = \log q_e - \frac{K_1}{2.303} t \quad (8)$$

$$\frac{t}{q_t} = \frac{1}{K_2 q_e^2} + \frac{1}{q_e} t \quad (9)$$

$$q_t = K_i t^{0.5} \quad (10)$$

$$\ln q_t = \ln A + B \ln t \quad (11)$$

where, q_e (mg/g) and q_t (mg/g) are the adsorption capacity at equilibrium and at time t (min), respectively, K_1 (1/min) is the rate constants of pseudo-first-order; K_2 (g/(mg·min)) is the rate constant of pseudo-second-order; k_i [mg/(g min^{0.5})] is the intraparticle diffusion rate constant; A and B are the double constant equation model constants. The kinetic constants and correlation coefficients for the models were calculated using the above equations and listed in Table 8 along with their R^2 value.

Results and discussions

XRD analysis. Figure 2a–c shows XRD patterns of bentonite, HAp, and bentonite/HAp samples, respectively. In Fig. 2c, the sharp and major peaks related to HAp were observed at $2\theta = 25.94, 28.7, 29.02, 31.77, 32.19, 32.90, 34.05, 35.48, 39.20, 39.8, 42.03, 43.80, 45.30, 46.71, 48.10, 48.62, \text{ and } 49.45$ are related to (002), (102), (210) (211), (112), (300), (301), (212), (310), (311), (113), (203), (222), (312), (320), and (213) planes, respectively. The positions and d -values matched well with (the JCPDS pattern 09–0432)³⁴. These peaks are also the same as those observed in Fig. 2b. However, the peaks at a $2\theta = 6.6^\circ, 20.1^\circ, 35.7^\circ, 54.1^\circ, \text{ and } 61.8^\circ$, which correspond to the (001), (100), (105), (210), (300) crystallographic planes, respectively (JCPDS No.12-0204)³⁵, confirmed the presence of bentonite clay in the composite. Similar peaks can be observed for pristine bentonite particles as shown in Fig. 2a. Therefore, the formation of the HAp/bentonite composite was corroborated by XRD analysis. The crystallite size was estimated by Scherrer's equation from the XRD pattern, $D = K\lambda/\beta\cos\theta$, where the constant k is 0.89, λ is the X-ray wavelength, β is the full-width half maximum and θ is the Bragg's angle. The crystallite sizes of HAp/bentonite were estimated to be 42.03 nm.

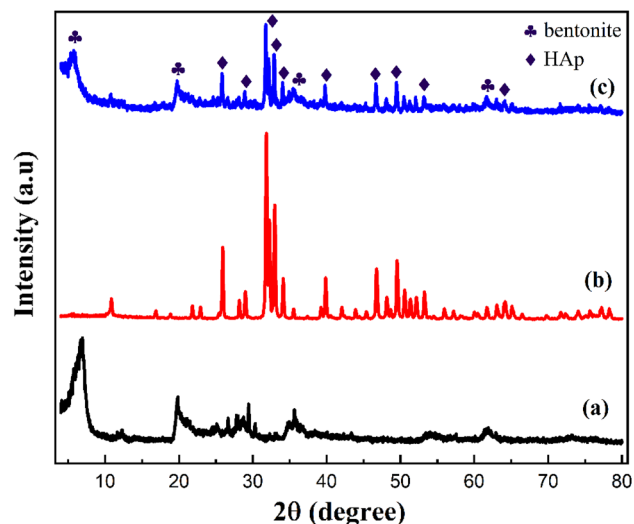


Figure 2. XRD pattern of (a) bentonite, (b) HAp, and (c) HAp/ bentonite composite.

SEM analysis. The surface morphology of bentonite, HAp/bentonite, and HAp/bentonite composite after adsorption of Cd(II) are shown in Fig. 3a–c, respectively. In Fig. 3a, the surface morphology of bentonite is a smooth surface with a fused and densely packed structure while the microstructure of HAp/bentonite composite revealed a rough and slightly porous surface. The SEM picture of HAp/bentonite also shows that the porous HAp aggregates are heterogeneously distributed over the surface of bentonite clay; hence, it provides more residence to the Cd(II) and has extra available bonding sites that facilitate the adsorption process. Figure 3c shows the morphology of the HAp/bentonite composite after Cd(II) adsorption. The morphology revealed an even greater degree of roughness on the surface due to the formation of thick assembly and adsorption of Cd(II).

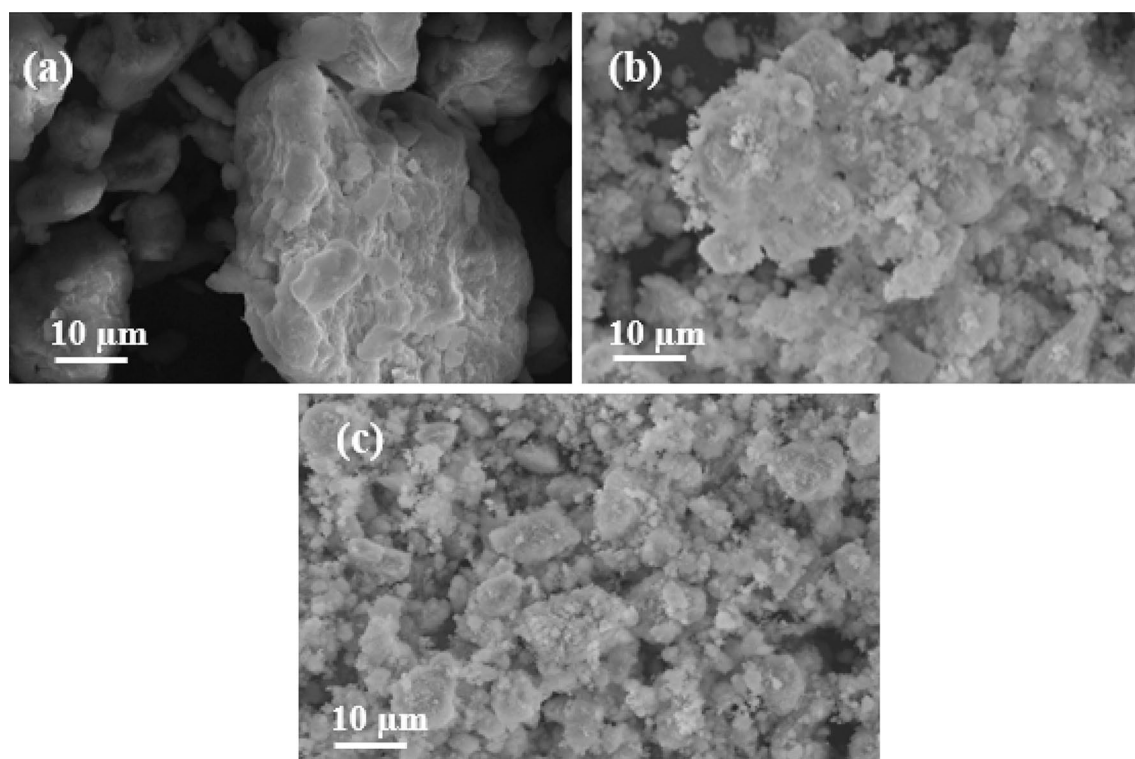


Figure 3. SEM image of (a) bentonite, (b) HAp/bentonite, and (c) HAp/bentonite composite after adsorption of Cd(II).

FTIR analysis. Figure 4a–d exhibits FTIR spectra of bentonite, HAp, HAp/bentonite, and HAp/bentonite composite after Cd(II) adsorption, respectively. Initially, the band around 1640 cm^{-1} and 3448 cm^{-1} were attributed to the hydroxyl group ($-\text{OH}$) stretching and bending, respectively in all samples. The number of water molecules present on the surface of the materials could be determined by their band intensity²⁷. As shown in Fig. 4a the intensity of the band was relatively lower for bentonite, which implies it has fewer bonded H_2O molecules. However, the peak of the band for HAp/bentonite composite was increased, which is credited to the presence of the large number of active hydroxyl groups on HAp/bentonite composite suggesting that the composite is favorable for the adsorption of Cd(II). The occurrence of PO_4^{3-} was indicated by the appearance of a band at 1037 cm^{-1} confirming the successful loading of HAp on the bentonite surface³⁶. A typical bentonite peak at 633 cm^{-1} , displayed the typical vibrations of alumina and silica-oxygen tetrahedral groups. Furthermore, the characteristic peak at $522\text{--}527\text{ cm}^{-1}$ indicates the presence of Si–O–Si bonds in HAp/bentonite composite³⁷. As shown in Fig. 4d the FTIR spectrum of the HAp/bentonite composite after Cd(II) adsorption was changed; the peaks at 3448 cm^{-1} and 1640 cm^{-1} attributed to the hydroxyl group ($-\text{OH}$) are relatively smaller than that of the sample before adsorption. This may be due to the complex formation between hydroxyl groups on the surface of HAp/bentonite and Cd(II) in solution³⁸. The peak at 3448 cm^{-1} was also shifted to 3427 cm^{-1} after adsorption this shift may be caused by the presence of O–Cd(II) bonds. Moreover, the peak of P–O at 1037 cm^{-1} gets weakened, suggesting that phosphate participated in the adsorption process of Cd(II).

BET analysis. The surface area was measured by absorption–desorption of nitrogen by the multipoint BET method. Concerning the textural properties, the composite presented a surface area of $257.27\text{ m}^2/\text{g}$ and was characterized as a mesoporous material. Theoretically, the observed high surface area is good in adsorption as it provides more active sites on the surface of the adsorbent. Table 2 revealed the BET surface area, pore volume, and pore size of the adsorbent.

Central composite design (CCD) and analysis of variance (ANOVA). CCD of the RSM approach was used to choose the effective model for the process and to optimize the adsorption process parameters^{39–41}. The experiments were performed as per the experimental design set by RSM (Table 3).

The analysis of variance (ANOVA) was applied to check the statistical adequacy of the quadratic model (Table 4). The significance of each term in the quadratic model is determined by the model F and P-values⁴². In general, a higher F-value and lower P-value of a variable revealed the significance of the model terms⁴³. According to the ANOVA results, the F-value for removing Cd(II) is 124.57 implies the model is statistically significant. Also, the P-value is less than 0.0500 indicating the model terms are significant. The coefficient of determination R^2 was found to be 0.9915 which is close to one, implying that 99.15% of the variability in the response can be explained by the quadratic model, and therefore only 0.85% of the observed variability is insignificant by the

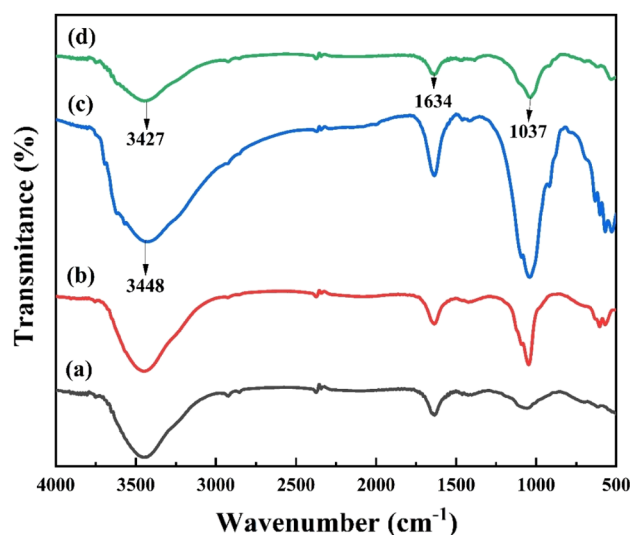


Figure 4. FTIR spectra of (a) bentonite, (b) HAp, (c) HAp/bentonite, and (d) HAp/bentonite after adsorption of Cd(II).

Adsorbent	BET surface area (m^2/g)	pore volume (cc/g)	pore diameter (nm)
HAp/bentonite	257.27	0.1621	7.92

Table 2. Textural properties of prepared HAp/bentonite adsorbent.

Independent variables Cd removal efficiency (% η)							
Std	Run	A	B	C	D	Efficiency	Predicted
19	1	75	0.25	5.5	50	74	73.65
15	2	50	1.75	6	60	94	95.39
6	3	100	0.75	6	40	78.5	79.18
18	4	125	1.25	5.5	50	77	76.35
16	5	100	1.75	6	60	92.3	92.47
3	6	50	1.75	5	40	94.5	95.89
4	7	100	1.75	5	40	90.3	90.07
30	8	75	1.25	5.5	50	98	97.25
27	9	75	1.25	5.5	50	96.5	97.25
14	10	100	0.75	6	60	81.5	81.37
17	11	25	1.25	5.5	50	87.9	88.06
29	12	75	1.25	5.5	50	97.5	97.25
26	13	75	1.25	5.5	50	97.5	97.25
25	14	75	1.25	5.5	50	96.5	97.25
2	15	100	0.75	5	40	74.6	74.47
1	16	50	0.75	5	40	84.2	83.27
13	17	50	0.75	6	60	87.8	87.27
7	18	50	1.75	6	40	97.3	95.95
28	19	75	1.25	5.5	50	97.5	97.25
23	20	75	1.25	5.5	30	91.9	91.88
9	21	50	0.75	5	60	84.8	85.70
21	22	75	1.25	4.5	50	88	87.93
20	23	75	2.25	5.5	50	97.5	97.36
8	24	100	1.75	6	40	92.3	92.65
5	25	50	0.75	6	40	84.7	85.45
24	26	75	1.25	5.5	70	94.6	94.13
11	27	50	1.75	5	60	97.4	95.95
22	28	75	1.25	6.5	50	92.5	92.08
12	29	100	1.75	5	60	90	90.50
10	30	100	0.75	5	60	76.7	77.28

Table 3. Batch mode adsorption process parameters used in RSM with the equivalent experimental and predicted values for the response.

model. Statistically, the difference between predicted R^2 and adjusted R^2 should be less than 0.2. In this case, the predicted R^2 of 0.9556 is in reasonable agreement with the adjusted R^2 of 0.9835; i.e., the difference is less than 0.2 and therefore is acceptable. Adequate precision measures the response values at the design space with the average prediction error, and a ratio greater than 4 is desirable. In this study, the Adeq precision is 34.1168 indicating an adequate signal, that can be used to navigate the design space. Besides the aforementioned results, a quadratic model is chosen to represent the interaction of the process variables as given in Eq. (10)⁴⁴.

$$\eta = 97.25 - 2.93A + 5.93B + 1.04C + 0.5625D + 0.7438AB + 0.6313AC - 0.5312BC - 0.5937BD - 3.76A^2 - 2.94B^2 - 1.81C^2 - 1.06D^2 \quad (12)$$

where η (%) is the removal efficiency of Cd(II), A is the initial concentration, B is the dosage of the adsorbent, C is the pH and D is the contact time.

To evaluate the selected model, an analysis of the residuals was performed. Residuals can be defined as the difference between the experimental and predicted value by the model⁴⁵. Figure 5a shows the normal probability versus externally studentized residuals for the removal efficiency of Cd(II). As can be seen, the residuals follow a straight line with no deviation. The plot shows a normal distribution of errors, confirming the significance of the selected models. In addition, Fig. 5b indicates a random scatter of residuals compared to the expected values. The plot revealed that the points distributed along a straight line, the significance of the model.

Effect of selected variables on the removal of Cd (II). The interaction of selected process parameters towards the adsorption of Cd(II) was investigated and shown in Fig. 6a–d. The interactive effect of the initial Cd(II) concentration and the adsorbent dose on the removal efficiency of the adsorbent was shown in Fig. 6a. From the 3D surface plot, it is clearly stated that the adsorption capacity decreased with increasing Cd(II) concentration. An increase in Cd(II) concentration from 50 to 100 mg/L with a 1.58 g/L dose resulted in a decrease in adsorptive removal from 99.3 to 80%. This could be attributed to the fact that the surface of the HAp/bentonite composite

Source	Sum of squares	df	Mean square	F-value	p-value	
Model	1685.60	14	120.40	124.57	<0.0001	Significant
A	205.92	1	205.92	213.06	<0.0001	
B	843.72	1	843.72	872.96	<0.0001	
C	25.83	1	25.83	26.73	0.0001	
D	7.59	1	7.59	7.86	0.0134	
AB	8.85	1	8.85	9.16	0.0085	
AC	6.38	1	6.38	6.60	0.0214	
AD	0.1406	1	0.1406	0.1455	0.7082	
BC	4.52	1	4.52	4.67	0.0472	
BD	5.64	1	5.64	5.84	0.0289	
CD	0.3906	1	0.3906	0.4042	0.5345	
A ²	388.08	1	388.08	401.53	<0.0001	
B ²	236.51	1	236.51	244.71	<0.0001	
C ²	90.00	1	90.00	93.12	<0.0001	
D ²	30.90	1	30.90	31.97	<0.0001	
Residual	14.50	15	0.9665			
Lack of fit	12.62	10	1.26	3.37	0.0963	Not significant
Pure error	1.88	5	0.3750			
Cor total	1700.10	29				

Table 4. ANOVA results for Cd removal using a quadratic model from CCD.

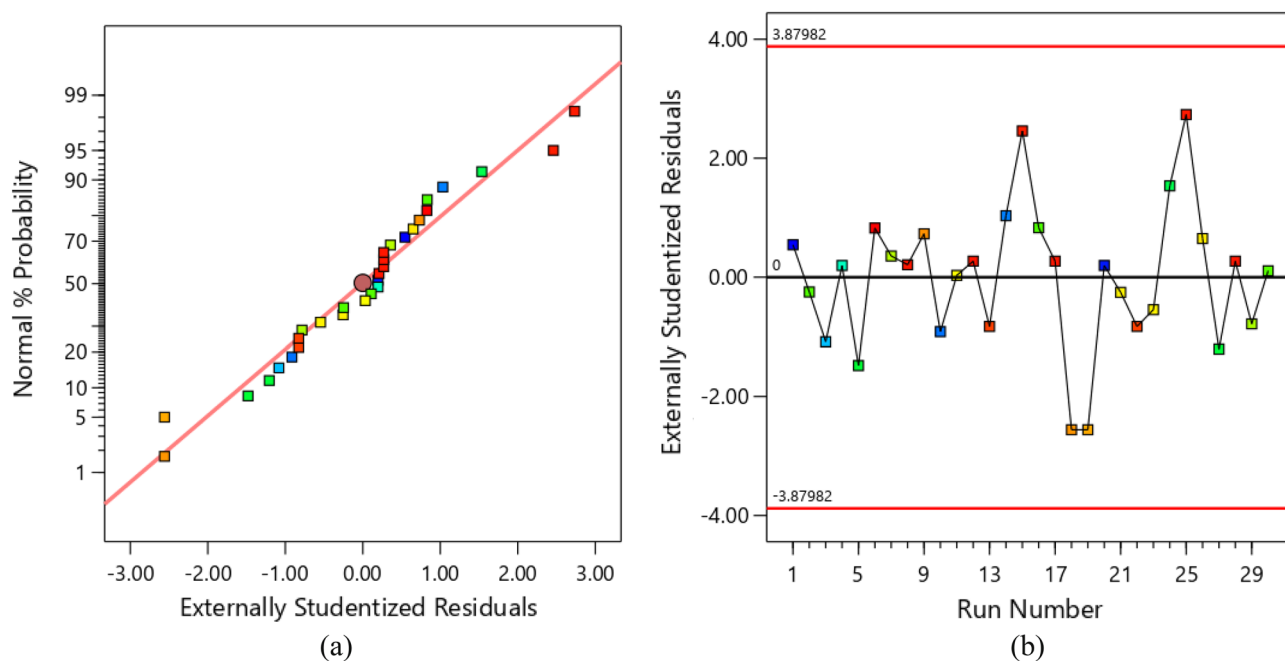


Figure 5. The normal plot of residuals (a), the plot of residuals versus run number for removal of Cd(II) (b).

becomes saturated in the presence of a higher concentration of Cd(II), eventually, the Cd(II) ion tends to form an aggregate on the outer surface of the composite and decreased the surface area. Similar results have been reported by Praipipat et al (2023), and the study showed that the removal efficiency was decreased with increasing concentration⁴⁶.

On the other hand, the sorption capacity increased with increasing the dosage of the composite⁴⁷. The probable reason is that when the adsorbent dose increases, the active sites of HAp/bentonite increase until all of the Cd(II) ions are adsorbed on the surface⁴⁸. These results are in line with Muhammad Shafiq et al. (2022), who studied the removal of Cd(II) from contaminated water using functionalized bentonite clay composite with NiAl-Layered Double Hydroxide. According to the obtained results, an increase in the uptake capacity of Cd (II) was observed by increasing the dosage of the adsorbents⁴⁹. Another result has been reported by Zongqiang Zhu et al. (2022), who investigated the removal of Cd(II) using Strontium-doped hydroxyapatite as an adsorbent. The effect

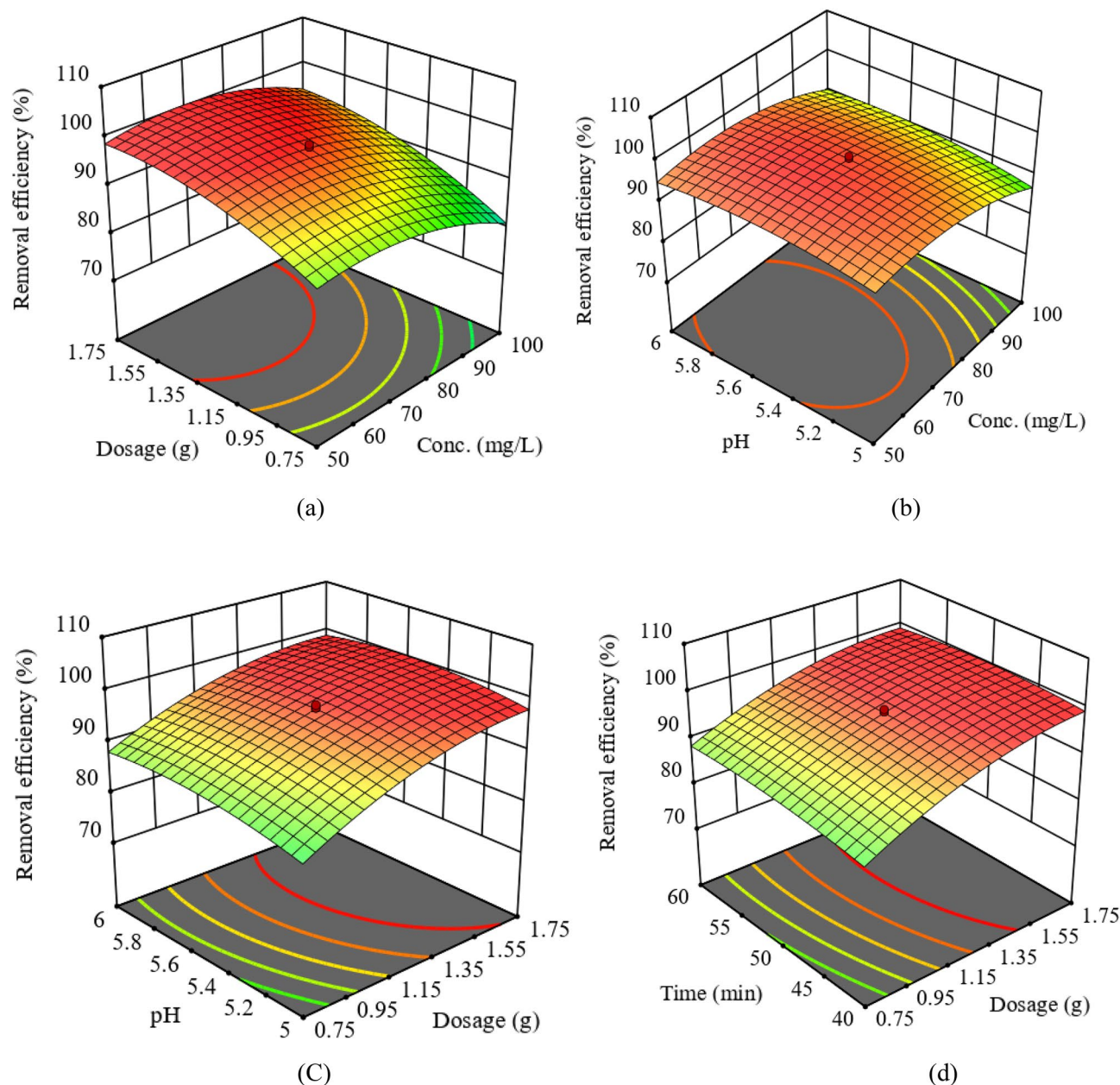


Figure 6. Interactive effect of parameters on the removal efficiency of Cd (II) (a) initial Cd concentration versus adsorbent dosage, (b) initial Cd concentration versus pH, (c) adsorbent dosage versus solution pH, and (d) adsorbent dosage versus contact time.

of adsorbent dosage, temperature, and an initial solution was studied. The result revealed that with increasing adsorbent dosage, the removal efficiency increased⁵⁰.

Figure 6b depicts the 3D plot of the initial Cd(II) concentration and the solution pH i.e., the pH has a positive effect on the removal efficiency. At a given pH of 5.8, an increase in Cd(II) concentration from 50 to 100 mg/L resulted in a decrease in the removal efficiency from 99.3 to 92%.

The 3D surface plot presented in Fig. 6c stated the effect of the adsorbent dose and the solution pH on Cd(II) removal. It was revealed that the removal efficiency increases with increasing the adsorbent dosage and the optimum dose was considered to be 1.58 g/L. From the 3D plot, it was also observed that the adsorptive removal efficiency increases from 90 to 99.3% upon increasing the pH. As can be seen from Fig. 10, the pHPzc of HAP/bentonite composite is 5.9. i.e., at pH < 5.9, the surface of the composite is positively charged and at pH > 5.9, the surface of the composite is negatively charged. Therefore, the removal efficiency decreases at pH < 5.9. This is because, at lower pH, Cd(II) and H⁺ ions compete to occupy the binding sites on the adsorbent surface, which leads to decreased adsorption capacity^{51,52}. On the contrary, in the basic medium, the surface HAP/bentonite composite becomes negatively charged, thereby decreasing the repulsive force. Although, with a further increase in pH, the Cd(II) tends to precipitate as Cd(OH)₂. These results found support from Abdelbaky Hossam Elgarhy

et al. (2022), who demonstrated that the removal percentage efficiency increased with increasing pH value. The findings further showed that the cation exchange capacity is strongly controlled by the pH of the solution⁵³.

Figure 6d presents the effect of varying the adsorbent dosage and contact time. At low contact time, the percentage removal of Cd(II) was fast. This is due to the presence of a pristine active site in the initial stage of adsorption followed by a slight increase in removal efficiency. However, the addition of time no longer increases the percentage removal after the contact time of 50 min, this is due to the active sites on the adsorbent becoming saturated by the Cd(II), and in time the Cd(II) detached from the surface of the adsorbent back into the solution⁵⁴. Hao Xu et al. (2020) obtained a similar result in their study to remove Cd(II) and Pb(II) using humic acid-iron-pillared bentonite. The result revealed that the adsorption capacity increased with the increase in contact time, reached a plateau region, and then slightly declined⁵⁵.

Optimization of removal of Cd (II) using RSM. The optimum values of the process parameters for the maximum Cd removal efficiency were determined as shown in Table 5 below. The experimental removal efficiency of HAp/bentonite at that optimal condition was proximate to the predicted value. This proves that the adopted method to optimize process parameters for maximum adsorption of Cd(II) onto HAp/bentonite composite is successful.

Adsorption equilibrium isotherm. Figure 7 depicts a comparison of the equilibrium data with the Langmuir and Freundlich isotherms to understand the sorption behavior⁵⁶. Table 6 suggests a better ($R^2 = 0.9889$) value for adsorption data of HAp/bentonite composite for the Langmuir adsorption isotherm model than the Freundlich model, thus, proving the homogeneous adsorbents. The separation factor R_L of the Langmuir isotherm model suggests the favorability of the adsorption system. The value of R_L should be comprised between 0 to 1 for favorable adsorption⁵⁷. In this study, the value of R_L was 0.05; confirming the applicability of the Langmuir isotherm. The maximum sorption capacity was found to be 125.47 mg/g and that was significantly higher compared to other adsorbents for Cd(II) removal from aqueous solutions as shown in Table 7.

Adsorption kinetics. The adsorption mechanism and rate were determined by the desired kinetic model, which in turn depends on the value of the correlation coefficient (R^2) for the linear mode of different kinetic equations. The kinetic parameters and their associated R^2 value are presented in Table 8, where R^2 was used to compare the fitting of the kinetic curves. Figure 8a shows a plot of $\log(q_e - q_t)$ versus t , and (t/q_t) versus t according to the pseudo-first-order and pseudo-second-order models, respectively. The low R^2 value of the pseudo-first-order model in Table 8 shows that the adsorption of the Cd(II) onto HAp/bentonite did not follow this model. However, the R^2 value of the pseudo-second-order model was found to be very close to 1.0. Furthermore, the estimated q_e value for the adsorption of Cd(II) found from the pseudo-second-order model is closer to the experimental q_e value, which suggests that the pseudo-second-order model fits the adsorption process. In Fig. 8b, the fit of the intraparticle diffusion model was determined by the plot of q_t versus $t^{0.5}$. The R^2 value was 0.5760 implying that the adsorption did not follow this model. In Fig. 8c, $\ln q_t$ was plotted versus $\ln t$ according to the double constant equation model. R^2 was also 0.6402, indicating that this model did not fit with the adsorption process. Therefore, it can be concluded that the adsorption of Cd(II) onto HAp/bentonite followed pseudo-second-order i.e., the rate involves forces for sharing or exchanging of electrons between Cd(II) and HAp/bentonite composite (chemisorption)⁶⁴.

Adsorption thermodynamics. To understand the nature of Cd(II) adsorption on HAp/bentonite, the thermodynamic parameters such as free energy change (ΔG), enthalpy changes (ΔH), and entropy change (ΔS) were investigated according to Van't Hof equation⁶⁵.

$$\Delta G = -RT \ln K_f \quad (13)$$

$$K_f = \frac{q_e}{C_e} \quad (14)$$

$$\ln K_f = -\frac{\Delta H}{RT} + \frac{\Delta S}{R} \quad (15)$$

where K_f (L/g) is called the distribution constant, q_e (mg/g) is the equilibrium adsorption capacity, C_e (mg/L) is the equilibrium concentration of the solution, T (K) is the absolute temperature, and R is the universal gas constant (8.314 J/mol K).

The Gibbs free energy (ΔG) of the adsorption reaction was calculated according to Eq. (11). Whereas the enthalpy change (ΔH) and the entropy change (ΔS) of adsorption were calculated from Van't Hoff plot of $\ln K$ vs

Optimized process parameters				Removal efficiency (η_p , %)		
Initial Concentration	Dosage	pH	Time	Predicted	Actual	Desirability
61.58	1.58	5.88	49.63	99.3	97.85	0.987

Table 5. Optimal conditions of the selected factors for Cd adsorption via HAp/bentonite.

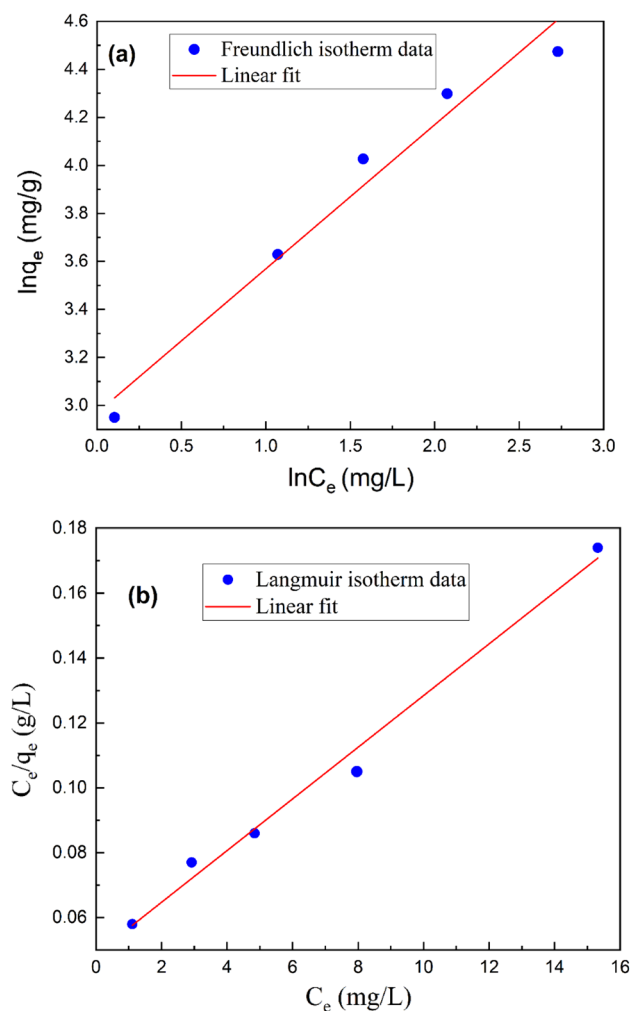


Figure 7. Freundlich (a) and Langmuir isotherms (b) for adsorption of Cd(II) onto HAp/bentonite composite.

Isotherm models	Parameters	Values	R^2
Freundlich	n	1.67	0.9700
	K_f (L/g)	19.47	
Langmuir	q_{max} (mg/g)	125.47	0.9889
	b (1/mg)	0.16	
	R_L	0.05	

Table 6. Parameters of Freundlich and Langmuir isotherms for adsorption of Cd(II) onto HAp/bentonite composite.

$1/T$ (Fig. 9). Thermodynamics results are shown in Table 9, where the positive value of ΔH indicates the adsorption process is endothermic due to the increase in adsorption upon a successive increase in the temperature. Negative values of ΔG indicate that the nature of Cd(II) adsorption is spontaneous and thermodynamically favorable. Moreover, the change in Gibbs free energy was inversely proportional to the temperature, and an increase in temperature enhanced the adsorption. ΔS value is negative, indicating that there is a higher disorder at the solid–the liquid interface during adsorption, which may be related to the ion exchange process⁶⁶.

The point of zero charge of HAp/bentonite composite. The point of zero charge is the pH at which the total surface charge of the adsorbent is neutral⁶⁷. In this study, the pH of the 0.01 M NaCl was adjusted to a value between 2 and 10 using 0.1 M HCl or 0.1 M NaOH. An adsorbent (0.5 g) was added to 50 mL of the pH-adjusted solution and stirred for 3 h on a shaker. Then, the pH of each solution was measured, and the diagram of the initial pH

Adsorbent	Maximum adsorption capacity (mg/g)	References
Ball clay	27.17	58
Bentonite-Fe ₃ O ₄ -MnO ₂	35.35	59
Composite of eggshell/starch/Fe ₃ O ₄	48.57	60
Thiol-modified bentonite (SH-Bent)	49.3	61
Nano-hydroxyapatite-modified biochar (HBC)	55.95	62
Amino-functionalized bentonite/CoFe ₂ O ₄ @MnO ₂	115.79	17
Hydroxyapatite-encapsulated zinc ferrite (HAp/ZnFe ₂ O ₄)	120.33	63
HAp/bentonite composite	125.47	Present study

Table 7. Comparison of maximum adsorption capacities of various adsorbents towards Cd(II).

Model	Parameters	Values	R ²
Pseudo-first-order	$q_{e,exper}$ (mg/g)	38.47	0.8866
	$q_{e,calc}$ (mg/g)	6.844	
	K_1 (min ⁻¹)	0.0350	
Pseudo-second-order	$q_{e,calc}$ (mg/g)	39.21	0.9985
	K_2 (min ⁻¹)	0.0111	
Intraparticle diffusion	K_i	0.5471	0.5760
Double constant equation model	A	30.081	0.6402
	B	0.0554	

Table 8. R² and constant values for different adsorption kinetics models of Cd(II) adsorption onto HAp/bentonite composite.

versus the final pH was plotted (Fig. 10). The pH where the two curves intersect is called pH_{pzc}, which is equal to 5.9 for HAp/bentonite.

Proposed mechanism for the adsorption process. As depicted in Fig. 4d, the FTIR peaks at 3440 cm⁻¹ and 1640 cm⁻¹ were reduced after Cd(II) on the composite, which implies surface complex formation between hydroxyl groups and Cd(II). Moreover, the adsorption peak of P–O at 1038 cm⁻¹ was changed, which proves that the role of the phosphate group of HAp was also significant. The adsorption of Cd(II) onto the HAp/bentonite surface relies on certain critical factors such as surface area, porosity, hydrogen bonding, electrostatic interactions between oppositely charged adsorbent surfaces and the adsorbate, etc²⁶. Furthermore, the solution pH also played a significant role by enhancing the deprotonation of binding sites and hence boosting the adsorption of Cd(II). The functional surface possessing phosphate groups exhibits a high affinity towards Cd(II) by electrostatic interactions in addition to the negatively charged bentonite layers⁶⁸. Generally, The possible adsorption mechanism of Cd(II) onto the HAp/bentonite was schematically explained as shown in Fig. 11.

Conclusion

The preparation and testing of a HAp/bentonite composite for the removal of Cd(II) from an aqueous solution were both successful. A facile synthesis route is reported in this study, which considers cost-effective material resources and environmental control. XRD, SEM, FTIR, and BET techniques were used to characterize the composite. The CCD-based RSM was used to optimize important process parameters such as initial Cd(II) concentration, adsorbent dosage, PH, and contact time. Based on the analysis of variance (ANOVA) result, the quadratic model was confirmed to describe the removal efficiency with a high correlation coefficient (R² = 0.9987). At optimal conditions, it was statistically optimized that 61.58 mg/L initial MO concentration, 1.58 g adsorbent dosage, 5.88 solution pH, and 49.63 min. contact time can achieve the maximum removal efficiency of 99.3%. Adsorption kinetics followed a pseudo-second-order kinetic model, indicating the chemisorption of Cd(II) on the surface of the composite. Equilibrium data were also best fitted with the Langmuir isotherm model, indicating that the surface active sites have an equal affinity towards Cd(II) ions. The maximum monolayer adsorption capacity was 125.47 mg/g, and the separation coefficient R_L was in the range of 0 to 1, indicating that HAp/bentonite was favorable for Cd (II) adsorption. Furthermore, thermodynamic studies illustrated that the adsorption of Cd(II) was a spontaneous and endothermic process. Meanwhile, the adsorption of Cd(II) onto HAp/bentonite is dependent on certain critical factors such as cation exchange, dissolution–precipitation, and surface complexation. In summary, the experimental results of this study showed that HAp/bentonite, which is

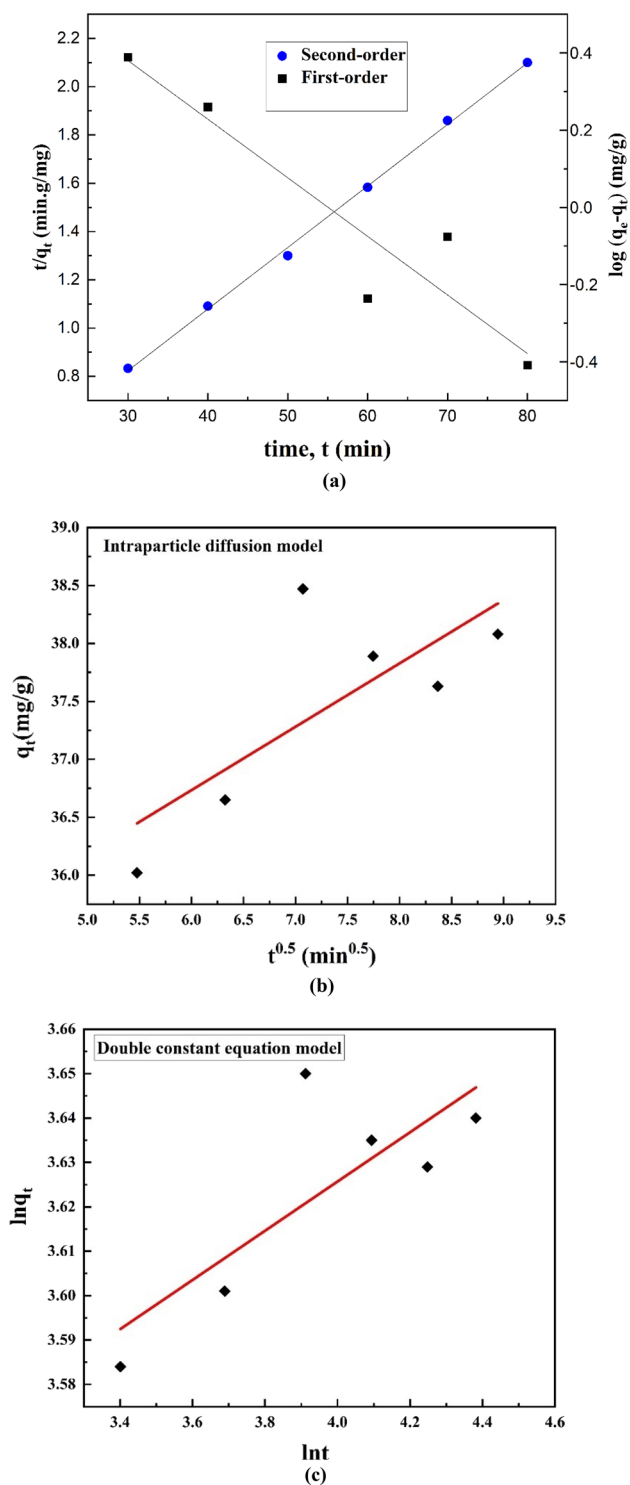


Figure 8. Linear fitting curves of adsorption kinetics. (a) Pseudo-first-order and pseudo-second-order kinetics models, (b) intraparticle diffusion model, and (c) double constant equation model for adsorption of Cd(II) onto HAp/bentonite composite.

safe, low-cost, environmentally friendly, and available material could be an effective adsorbent with optimized process parameters by CCD to remove Cd(II) from contaminated water.

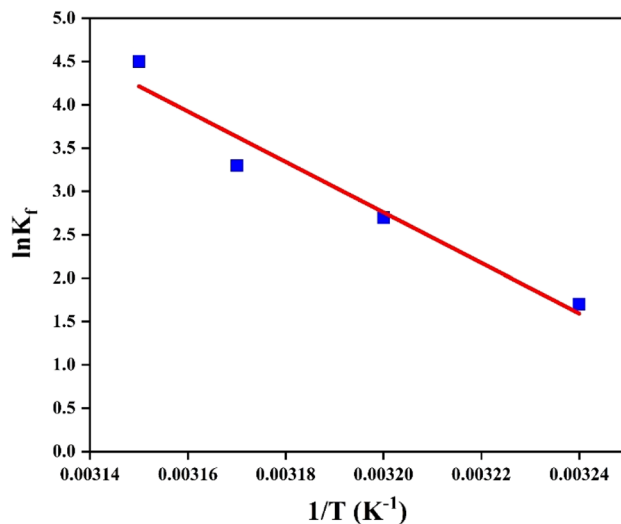


Figure 9. Adsorption thermodynamics of Cd(II) onto HAp/bentonite composite.

Adsorbent	ΔH (kJ/mol)	ΔS (Jmol/K)	ΔG (kJ/mol)			
			25 °C	35 °C	45 °C	55 °C
HAp/bentonite	7148	254.10	-4.24	-6.78	-9.32	-11.86

Table 9. Thermodynamic parameters of the adsorption of Cd(II) onto HAp/bentonite.

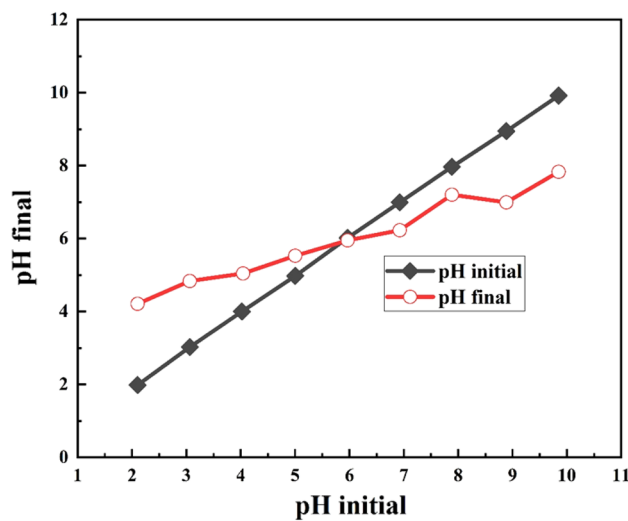


Figure 10. The pH_{pzc} of HAp/bentonite.

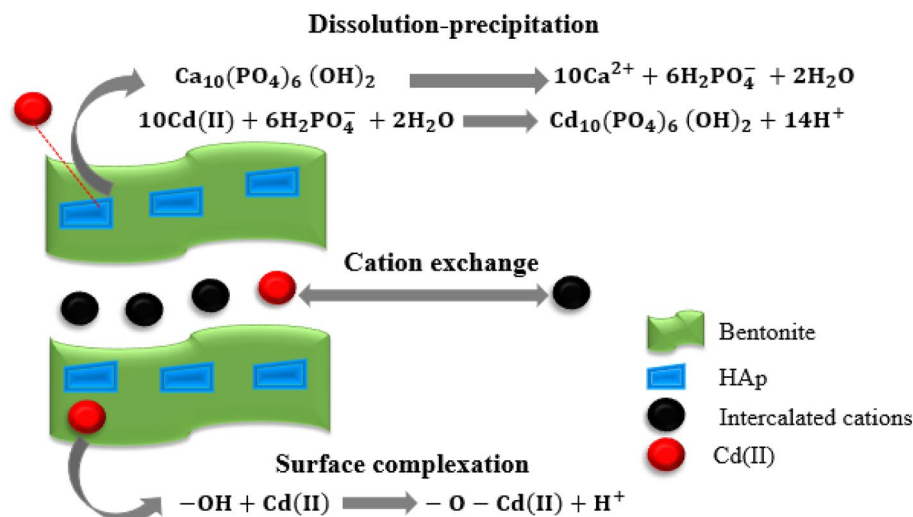


Figure 11. The possible mechanism of Cd(II) adsorption on HAp/bentonite composite.

Data availability

The datasets generated during and/or analyzed during the current study are available from the corresponding author on reasonable request.

Received: 20 January 2023; Accepted: 27 March 2023

Published online: 29 March 2023

References

- Shrestha, R. *et al.* Technological trends in heavy metals removal from industrial wastewater: A review. *J. Environ. Chem. Eng.* **9**(4), 105688 (2021).
- Chai, W. S. *et al.* A review on conventional and novel materials towards heavy metal adsorption in wastewater treatment application. *J. Clean. Prod.* **296**, 126589 (2021).
- Muhammad, S. & Usman, Q. A. Heavy metal contamination in water of Indus River and its tributaries, Northern Pakistan: Evaluation for potential risk and source apportionment. *Toxin Rev.* **41**(2), 380–388 (2022).
- Haider, F. U. *et al.* Cadmium toxicity in plants: Impacts and remediation strategies. *Ecotoxicol. Environ. Saf.* **211**, 111887 (2021).
- Abdollahi, S. A., Mokhtariyan, N. & Ameri, C. Design, synthesis and application of a sponge-like nanocomposite ceramic for the treatment of Ni (II) and Co (II) wastewater in the zinc ingot industry. *Arab. J. Chem.* **15**(1), 103477 (2022).
- Xu, Y. *et al.* Chronic cadmium exposure at environmental-relevant level accelerates the development of hepatotoxicity to hepatocarcinogenesis. *Sci. Total Environ.* **783**, 146958 (2021).
- Awual, M. R. *et al.* Efficient detection and adsorption of cadmium (II) ions using innovative nano-composite materials. *Chem. Eng. J.* **343**, 118–127 (2018).
- Othmani, A. *et al.* Agricultural waste materials for adsorptive removal of phenols, chromium (VI) and cadmium (II) from wastewater: A review. *Environ. Res.* **204**, 111916 (2022).
- Duan, C. *et al.* Removal of heavy metals from aqueous solution using carbon-based adsorbents: A review. *J. Water Process Environ.* **37**, 101339 (2020).
- Liu, T. *et al.* Adsorption of cadmium and lead from aqueous solution using modified biochar: A review. *J. Environ. Chem. Eng.* **10**(1), 106502 (2022).
- El Malti, W. *et al.* Comparative study of the elimination of copper, cadmium, and methylene blue from water by adsorption on the citrus Sinensis peel and its activated carbon. *RSC Adv.* **12**(17), 10186–10197 (2022).
- Uddin, M. K., Rao, R. A. K. & Mouli, K. V. C. The artificial neural network and Box–Behnken design for Cu²⁺ removal by the pottery sludge from water samples: Equilibrium, kinetic and thermodynamic studies. *J. Mol. Liq.* **266**, 617–627 (2018).
- Guan, X. *et al.* Adsorption behaviors and mechanisms of Fe/Mg layered double hydroxide loaded on bentonite on Cd (II) and Pb (II) removal. *J. Colloid Interface Sci.* **612**, 572–583 (2022).
- Elkhatib, E. A. *et al.* Using nano-magnesium oxide/bentonite composite for cadmium removal from industrial wastewater. *Environ. Eng. Res.* **28**(2), 210545 (2022).
- Hend, H. *et al.* Dynamic removal of cumulative toxic heavy metals Pb (II) and Cd (II) from aqueous solutions via activated nano-sized bentonite adsorbents. *Int. J. Contemp. Appl. Sci* **3**, 67–82 (2016).
- Şahan, T. Application of RSM for Pb(II) and Cu(II) adsorption by bentonite enriched with SH groups and a binary system study. *J. Water Process Eng.* **31**, 100867 (2019).
- Zhou, G. *et al.* Synthesis of amino-functionalized bentonite/CoFe₂O₄@ MnO₂ magnetic recoverable nanoparticles for aqueous Cd²⁺ removal. *Sci. Total Environ.* **682**, 505–513 (2019).
- Yan, Y. *et al.* Green synthesized hydroxyapatite for efficient immobilization of cadmium in weakly alkaline environment. *Environ. Res.* **223**, 115445 (2023).
- Ofudje, E. A. *et al.* Adsorption of Cd²⁺ onto apatite surface: Equilibrium, kinetics and thermodynamic studies. *Heliyon.* **9**, e12971 (2023).
- Núñez, D. *et al.* Heavy metal removal from aqueous systems using hydroxyapatite nanocrystals derived from clam shells. *RSC Adv.* **9**(40), 22883–22890 (2019).
- Oni, O. P. *et al.* Syntheses and applications of mesoporous hydroxyapatite: A review. *Mater. Chem. Front.* **7**, 1 (2023).
- Wang, M. *et al.* Adsorption behaviors and mechanisms of simultaneous cadmium and fluoride removal on waste bovine bone from aqueous solution. *J. Environ. Chem. Eng.* **11**(1), 109035 (2023).

23. Hong, C. *et al.* Effectiveness and mechanism for the simultaneous adsorption of Pb (II), Cd (II) and As (III) by animal-derived biochar/ferrhydrite composite. *Chemosphere* **293**, 133583 (2022).
24. Googerdchian, F. *et al.* Optimization of Pb (II) ions adsorption on nanohydroxyapatite adsorbents by applying Taguchi method. *J. Hazard Mater.* **349**, 186–194 (2018).
25. Trakoolwannachai, V., Kheolamai, P. & Ummartyotin, S. Characterization of hydroxyapatite from eggshell waste and polycaprolactone (PCL) composite for scaffold material. *J. Compos. Part B Eng.* **173**, 106974 (2019).
26. Guo, Y. *et al.* Efficient removal of uranium (VI) by 3D hierarchical Mg/Fe-LDH supported nanoscale hydroxyapatite: A synthetic experimental and mechanism studies. *Chem. Eng. J.* **392**, 123682 (2020).
27. Desalegn, Y. M., Andoshe, D. M. & Desissa, T. D. J. Composite of bentonite/CoFe₂O₄/hydroxyapatite for adsorption of Pb (II). *Mater. Res. Exp.* **7**(11), 115501 (2020).
28. Walsh, K. *et al.* Equilibrium data and its analysis with the Freundlich model in the adsorption of arsenic(V) on granular ferric hydroxide. *Sep. Purif. Technol.* **243**, 116704 (2020).
29. Romero-González, J. *et al.* Potential of *Agave lechuguilla* biomass for Cr(III) removal from aqueous solutions: Thermodynamic studies. *Biores. Technol.* **97**(1), 178–182 (2006).
30. Al-Ghouti, M. A. & Da'ana, D. A. Guidelines for the use and interpretation of adsorption isotherm models: A review. *J. Hazard Mater.* **393**, 122383 (2020).
31. Zhao, X. *et al.* Effect and mechanisms of synthesis conditions on the cadmium adsorption capacity of modified fly ash. *Ecotoxicol. Environ. Saf.* **223**, 112550 (2021).
32. Saleh, A., Sari, T. A. & Tuzen, M. Chitosan-modified vermiculite for As(III) adsorption from aqueous solution: Equilibrium, thermodynamic and kinetic studies. *J. Mol. Liq.* **219**, 937–945 (2016).
33. Bouchelkia, N. *et al.* Jujube stones based highly efficient activated carbon for methylene blue adsorption: Kinetics and isotherms modeling, thermodynamics and mechanism study, optimization via response surface methodology and machine learning approaches. *Process Saf. Environ. Prot.* **170**, 513–535 (2023).
34. Ashokan, A. *et al.* Eggshell derived hydroxyapatite microspheres for chromatographic applications by a novel dissolution-precipitation method. *Ceram. Int.* **47**(13), 18575–18583 (2021).
35. Zhou, G. *et al.* Synthesis of amino-functionalized bentonite/CoFe₂O₄@ MnO₂ magnetic recoverable nanoparticles for aqueous Cd²⁺ removal. *Nanomaterials* **682**, 505–513 (2019).
36. Sinulingga, K. *et al.* Synthesis and characterizations of natural limestone-derived nano-hydroxyapatite (HAP): A comparison study of different metals doped HAPs on antibacterial activity. *RSC Adv.* **11**(26), 15896–15904 (2021).
37. Rasheed, U. *et al.* Modification of bentonite with orange peels extract and its application as mycotoxins' binder in buffered solutions and simulated gastrointestinal fluids. *J. Clean. Prod.* **267**, 122105 (2020).
38. Han, X. *et al.* Enhanced Cr (VI) removal from water using a green synthesized nanocrystalline chlorapatite: Physicochemical interpretations and fixed-bed column mathematical model study. *Chemosphere* **264**, 128421 (2021).
39. Yusuff, A. S. Optimization of adsorption of Cr (VI) from aqueous solution by *Leucaena leucocephala* seed shell activated carbon using design of experiment. *Appl. Water Sci.* **8**(8), 1–11 (2018).
40. Sasidharan, R. & Kumar, A. J. Response surface methodology for optimization of heavy metal removal by magnetic biosorbent made from anaerobic sludge. *J. Indian Chem. Soc.* **99**(9), 100638 (2022).
41. Masoumi, H., Ghaemi, A. & Gilani, H. G. Synthesis of polystyrene-based hyper-cross-linked polymers for Cd (II) ions removal from aqueous solutions: Experimental and RSM modeling. *J. Hazard Mater.* **416**, 125923 (2021).
42. Bayuo, J. *et al.* Response surface optimization and modeling in heavy metal removal from wastewater—A critical review. *Environ. Monit. Assess.* **194**(5), 1–34 (2022).
43. Zhao, X. *et al.* Experimental modelling studies on the removal of dyes and heavy metal ions using ZnFe₂O₄ nanoparticles. *Sci. Rep.* **12**(1), 5987 (2022).
44. Uddin, M. K. & Nasar, A. Walnut shell powder as a low-cost adsorbent for methylene blue dye: Isotherm, kinetics, thermodynamic, desorption and response surface methodology examinations. *Sci. Rep.* **10**(1), 7983 (2020).
45. Sun, X. *et al.* Retracted Article: Optimization of dyes and toxic metals removal from environmental water samples by clinoptilolite zeolite using response surface methodology approach. *Sci. Rep.* **12**(1), 13218 (2022).
46. Praipipat, P., Ngamsurach, P. & Roopkhan, N. Zeolite A powder and beads from sugarcane bagasse fly ash modified with iron (III) oxide-hydroxide for lead adsorption. *Sci. Rep.* **13**(1), 1873 (2023).
47. Desalegn, Y. M. *et al.* Optimization of adsorption of methyl orange from aqueous solution by magnetic CoFe₂O₄/ZnAl-layered double hydroxide composite using response surface methodology. *Mater. Res. Exp.* **35**, 1 (2023).
48. Xu, H. *et al.* Cd (II) and Pb (II) adsorbed on humic acid-iron-pillared bentonite: Kinetics, thermodynamics and mechanism of adsorption. *Colloids Surf. A Physicochem. Eng. Asp.* **612**, 126005 (2021).
49. Shafiq, M., Alazba, A. A. & Amin, M. T. Functionalized bentonite clay composite with NiAl-layered double hydroxide for the effective removal of Cd (II) from contaminated water. *Sustainability* **14**(22), 15462 (2022).
50. Zhu, Z. *et al.* Strontium-doped hydroxyapatite as an efficient adsorbent for Cd (II) removal from wastewater: Performance, kinetics, and mechanism. *Environ. Technol. Innov.* **28**, 102575 (2022).
51. Li, D. *et al.* Adsorption of Cd(II) by synthetic zeolite under multi-factor using response surface methodology. *Colloids Surf. A Physicochem. Eng. Asp.* **647**, 129165 (2022).
52. Ecer, Ü. *et al.* Highly efficient Cd (II) adsorption using mercapto-modified bentonite as a novel adsorbent: An experimental design application based on response surface methodology for optimization. *Water Sci. Technol.* **78**(6), 1348–1360 (2018).
53. Elgarhy, A. H. *et al.* Comparative study for removal of phosphorus from aqueous solution by natural and activated bentonite. *Sci. Rep.* **12**(1), 19433 (2022).
54. Aniagor, C. O. *et al.* Equilibrium and kinetic modelling of aqueous cadmium ion and activated carbon adsorption system. *Water Conserv. Sci. Technol.* **6**(2), 95–104 (2021).
55. Xu, H. *et al.* Cd (II) and Pb (II) adsorbed on humic acid-iron-pillared bentonite: Kinetics, thermodynamics and mechanism of adsorption. *Colloids Surf. A* **612**, 126005 (2021).
56. Foroutan, R. *et al.* Hydroxyapatite biomaterial production from chicken (femur and beak) and fishbone waste through a chemical less method for Cd²⁺ removal from shipbuilding wastewater. *J. Hazard Mater.* **413**, 125428 (2021).
57. Shan, R.-R. *et al.* Magnetic Fe₃O₄/MgAl-LDH composite for effective removal of three red dyes from aqueous solution. *Chem. Eng. J.* **252**, 38–46 (2014).
58. Rao, R. A. K. & Kashifuddin, M. Adsorption studies of Cd(II) on ball clay: Comparison with other natural clays. *Arab. J. Chem.* **9**, S1233–S1241 (2016).
59. Jiang, L. *et al.* Preparation of magnetically recoverable bentonite-Fe₃O₄-MnO₂ composite particles for Cd (II) removal from aqueous solutions. *J. Colloid Interface Sci.* **513**, 748–759 (2018).
60. Hosseini, S. S. *et al.* Decontamination of Cd²⁺ and Pb²⁺ from aqueous solution using a magnetic nanocomposite of eggshell/starch/Fe₃O₄. *J. Water Process Eng.* **48**, 102911 (2022).
61. Song, R. *et al.* Improved adsorption and desorption behavior of Cd on thiol-modified bentonite grafted with cysteamine hydrochloride. *Res. Chem. Intermed.* **48**(6), 2721–2744 (2022).
62. Zhu, S. *et al.* The distinctive role of nano-hydroxyapatite modified biochar for alleviation of cadmium and arsenic toxicity in aqueous system. *J. Water Process Eng.* **49**, 103054 (2022).

63. Das, K. C. & Dhar, S. S. Removal of cadmium (II) from aqueous solution by hydroxyapatite-encapsulated zinc ferrite (HAP/ZnFe₂O₄) nanocomposite: kinetics and isotherm study. *Environ. Sci. Pollut. Res.* **27**(30), 37977–37988 (2020).
64. Zaghoul, A. *et al.* Characterization and application of MgAl layered double hydroxide for methyl orange removal from aqueous solution. *Mater. Today Proc.* **37**, 3793–3797 (2021).
65. Ebisike, K. *et al.* Thermodynamic study of the adsorption of Cd²⁺ and Ni²⁺ onto chitosan–silica hybrid aerogel from aqueous solution. *Results Chem.* **5**, 100730 (2023).
66. Wang, Y. *et al.* Adsorptive removal of tetracycline by sustainable ceramsite substrate from bentonite/red mud/pine sawdust. *Sci. Rep.* **10**(1), 1–18 (2020).
67. Algamdi, M., Alshahrani, A. & Alsuhaybi, M. Chitosan grafted tetracarboxylic functionalized magnetic nanoparticles for removal of Pb (II) from an aqueous environment. *Int. J. Biol. Macromol.* **225**, 1517–1528 (2023).
68. Jung, K.-W. *et al.* A facile one-pot hydrothermal synthesis of hydroxyapatite/biochar nanocomposites: Adsorption behavior and mechanisms for the removal of copper (II) from aqueous media. *Chem. Eng. J.* **369**, 529–541 (2019).

Author contributions

Y.M.D. and E.A.B. conducted the experiments; Y.M.D. analyzed, interpreted the data, and wrote the manuscript with support from F.E.O. F.E.O. edited the manuscript. All authors reviewed the manuscript.

Competing interests

The authors declare no competing interests.

Additional information

Correspondence and requests for materials should be addressed to Y.M.D.

Reprints and permissions information is available at www.nature.com/reprints.

Publisher's note Springer Nature remains neutral with regard to jurisdictional claims in published maps and institutional affiliations.



Open Access This article is licensed under a Creative Commons Attribution 4.0 International License, which permits use, sharing, adaptation, distribution and reproduction in any medium or format, as long as you give appropriate credit to the original author(s) and the source, provide a link to the Creative Commons licence, and indicate if changes were made. The images or other third party material in this article are included in the article's Creative Commons licence, unless indicated otherwise in a credit line to the material. If material is not included in the article's Creative Commons licence and your intended use is not permitted by statutory regulation or exceeds the permitted use, you will need to obtain permission directly from the copyright holder. To view a copy of this licence, visit <http://creativecommons.org/licenses/by/4.0/>.

© The Author(s) 2023